

© 2019. This manuscript version is made available under the CC-BY-NC-ND 4.0 license  
<https://creativecommons.org/licenses/by-nc-nd/4.0/>

This is the postprint version of an article accepted for publication in Nuclear Instruments and Methods in Physics Research Section B: Beam Interactions with Materials and Atoms (Elsevier). The Version of Record is available online at  
<https://doi.org/10.1016/j.nimb.2019.11.009>

## **Ion beam induced transient amorphous nucleation in silicon**

Corrado Spinella<sup>1</sup>, Stefania M.S. Privitera<sup>1</sup>, Antonio Massimiliano Mio<sup>1,\*</sup>, Emanuele Rimini<sup>1,2</sup>

1. Istituto per la Microelettronica e Microsistemi – Consiglio Nazionale delle Ricerche, Zona Industriale VIII Strada 5, 95121 Catania, Italy

2. Dipartimento di Fisica e Astronomia, Università di Catania, via S. Sofia 64, I-95123 Catania, Italia

\*Corresponding Author: [antonio.mio@imm.cnr.it](mailto:antonio.mio@imm.cnr.it)

**Keywords:** Materials analysis & modification by accelerators, Monte Carlo methods, Irradiation, Amorphous semiconductors, Defects, Growth, Nucleation

### **Abstract**

Ion-beam amorphization of crystalline silicon is reviewed. All the peculiar features of the process (temperature effect, incubation fluence, superlinear behavior of the amorphous fraction as a function of the ion fluence, dose–rate effects, ion mass/energy dependence, doping influence, etc.) can be explained within the classical theory of nucleation and growth based on capillarity. Nucleation and growth rates depend on the free energy of the amorphous clusters and on the kinetics balance between damage creation at the prompt stage of each ion collision cascade and competitive re–crystallization induced by atomic jumps of long living defects at the cluster surface. The model explains the damage accumulation kinetics either in dilute or dense collision cascade. It

is an extension of the theoretical approach describing the reverse process, i.e. the ion–beam assisted nucleation and growth of crystalline clusters in the amorphous material. The description is independent on the atomistic nature of the involved defects.

## 1. Introduction

Amorphization of silicon by ion beam irradiation occurs in many fabrication steps in the silicon–based device technology [1]. It can be a desired process, such as the pre–amorphizing implants to form highly doped shallow regions [2] in nanometric–scale silicon devices or to promote the Si reaction in silicide metallic contacts [3,4], or it can be a side effect in highly doped regions. The experimental data on the silicon amorphization induced by ion–beam irradiation show that the process is the result of a competition between damage generation and its dynamic annihilation, mainly governed by the temperature dependent defect mobility. The evolution of amorphous fraction is then critically dependent on substrate temperature, on the energy deposited by the ion into elastic collisions, on dose rate, and on dopant concentration. An exhaustive review of all of these evidences can be found in Ref. [5] for the Silicon amorphization and in Ref. [6, 7] for compound semiconductors. Recently, the role of defect diffusion during the dynamic annealing in ion-irradiated Si has been investigated by means of pulsed beam irradiation [8, 9]. The process is governed by interstitial and vacancy migration characterized by different activation energies. The dynamic annealing rate is limited by vacancy annihilation at sinks and by divacancy formation.

Compound semiconductors differ noticeable for their response to irradiation, since the transition to the amorphous phase is quite complex. It has been shown that the cross section of damage production is not correlated to the ionicity, nor to the elastic constants of the materials. A correlation has been found instead with the force constant associated to the optical lattice vibrations [10]. A similar view [11] has been adopted to describe the resistance of different compounds to

amorphization by radiation damage. The behavior in the analyzed compounds is determined by the competition between the short-range covalent and long –range ionic forces. With increasing the role of the covalent force to the total force the resistance to amorphization decreases. Due to the complexity of the considered phenomenon the reported investigation is then related only to silicon.

Although many attempts have been made to theoretically describe the amorphization process, no single model, however, appears to be able to explain all the huge amount of experimental data. It has been proposed that amorphization of silicon can be described either by a homogeneous or by an heterogeneous process. In the first case amorphization occurs when the lattice energy density overcomes a critical value (critical energy/defect model) [12,13]. In the second case amorphization results as a consequence of the overlapping of locally disordered regions within each ion collision cascade (overlap damage model) [14,15]. More recently, a fully atomistic model, based on the assumption that the interstitial–vacancy (IV) pair is the elementary unit forming amorphous embryos, has been proposed, suggesting the existence of a critical radius related to the stability of such complexes, whose recombination is characterized by different activation energies depending on their degree of coordination [16].

In the present paper we model silicon amorphization under ion irradiation in terms of ion–beam induced nucleation and growth of amorphous clusters, by following classical theory based on capillarity. The main assumption is that any single incident ion creates in the crystal lattice two different types of defects during the prompt stage of its collision cascade. The ions generate: *i*) vacancies, interstitials, vacancy–interstitial pairs, divacancies etc, causing formation and growth of the amorphous phase, and *ii*) long–living (e.g. dangling–bond–like) defects, responsible of damage recovering. The concentration of these latter defects progressively increases during irradiation and, for temperatures at which where amorphization is observed, it remains far from its steady–state

value for a significant fraction of time, giving rise to a transient behavior of the crystal to amorphous transition.

The model accounts for the detailed dependence of the amorphous fraction on the irradiation fluence in a wide range of irradiation parameters (ion mass, energy, dose rate) and of target temperature. The description evidences the existence of an incubation time associated with the formation of supercritical stable amorphous clusters. For large cluster sizes, the model converges to the theoretical description that explains the behavior of the ion–beam induced planar crystallization/amorphization (IBIEC) [17], and moreover it can be seen as an obvious extension of the theoretical approach adopted to describe the reverse process, i.e. the ion–beam assisted nucleation and growth of crystalline clusters in the amorphous material [18, 19]. The model, as already said, does not describe, from the atomistic point of view, the amorphous formation, i. e. the transition of point defects, such as vacancy, interstitials, divacancies, interstitial-vacancy pair and small agglomerates into amorphous cluster.

## 2. Theoretical description

Silicon amorphization is modeled by extending the formalism previously developed to describe ion–beam assisted crystal grain nucleation and growth [18, 19]. The impinging of the  $j$ -th ion on the area defined by its collision cascade of radius  $r_0$  generates during the life of the collision cascade, the prompt stage,  $\Delta t_{\text{prompt}}$  ( $\sim 0.1 \div 1$  ps), defects like self–interstitials, vacancies, and interstitial–vacancies pairs. Our description does not need to take into account for the detailed atomistic structure of these defects. A plethora of defects are created by the irradiation; in addition, their interaction depends also on their concentration and on the state of the surrounding material. There are in literature several attempts to develop atomistic models to describe the ion beam

induced amorphization of silicon. The situation is so complex that neither the experiments nor the simulations allow a clear identification of the atomistic nature of the involved defects to describe the amorphous formation. For these reasons the only assumption we make is that such defects, during the prompt stage prior to disappear, convert a certain concentration  $n_0$  of crystal atoms in the amorphous state, leading to the nucleation and growth of amorphous clusters.

At any instant  $t$  the concentration  $N_{i,t}$  of clusters with  $i$  atoms in the amorphous phase will increase accordingly to the following rate equations:

$$\frac{\partial N_{i,t}}{\partial t} = k_{i-1}^{\alpha} N_{i-1,t} - k_i^{\alpha} N_{i,t} \quad i = 1, 2, 3, \dots, i_{\max} \quad (1a)$$

$$N_{0,t} = \rho - \sum_{i=1}^{i_{\max}} i N_{i,t} \quad (1b)$$

where  $N_{0,t}$  is the concentration of monomers in the crystal phase,  $k_i^{\alpha}$  the number of atoms converted in the amorphous phase per second at the surface of clusters with size  $i$  and  $\rho$  the silicon atomic density. Under the hypothesis that the concentration  $n_0$  of atoms converted into the amorphous state by the ion beam is also trapped at the cluster surface, the transition rate  $k_i^{\alpha}$  will be proportional to  $n_0/\Delta t_{\text{prompt}}$  and to the number  $O_i$  of atoms at the cluster surface:

$$k_i^{\alpha} = A(1 - \chi_t) \frac{n_0}{\Delta t_{\text{prompt}}} O_i \quad (2)$$

here  $\chi_t$  is the amorphous fraction at the instant  $t$  that is related to  $N_{0,t}$  through the following relationship:

$$\chi_t = 1 - \frac{N_{0,t}}{\rho} \quad (3)$$

The term  $(1 - \chi_t)$ , introduced in Eq. 2, takes into account for the reduced availability of crystal atoms that can be converted into the amorphous state while the clusters grow.

The parameter  $A$  is determined by imposing that the total number of atoms converted into the amorphous phase per unit time at the surface of all the clusters is equal to  $(1 - \chi_t) \frac{n_0}{\Delta t_{\text{prompt}}}$ , i.e.:

$$\sum_{i=0}^{i_{\max}} k_i^\alpha N_{i,t} = \sum_{i=0}^{i_{\max}} A(1 - \chi_t) \frac{n_0}{\Delta t_{\text{prompt}}} O_i N_{i,t} = (1 - \chi_t) \frac{n_0}{\Delta t_{\text{prompt}}} \quad (4)$$

and then:

$$A = \frac{1}{\sum_{i=0}^m O_i N_{i,t}} \quad (5)$$

Assuming spherically shaped clusters, the number of atoms  $O_i$  at the amorphous–crystal interface depends on the cluster size  $i$  through the following relationship:

$$O_i = 4\pi \left( \frac{3}{4\pi} \right)^{2/3} i^{2/3} \quad \text{for } i > 0 \quad (6)$$

further, we impose  $O_i = 1$  for  $i = 0$ , the size conventionally attributed to the monomers in their initial crystal phase.

By introducing the dimensionless variable  $\xi = t/\Delta t_{\text{prompt}}$ , Eqs. 1a and 1b become:

$$\frac{\partial N_{i,\xi}}{\partial \xi} = An_0(1 - \chi_\xi)(O_{i-1}N_{i-1,\xi} - O_iN_{i,\xi}) \quad i = 1, 2, 3, \dots, i_{\max} \quad (7a)$$

$$N_{0,\xi} = \rho - \sum_{i=1}^{i_{\max}} iN_{i,\xi} \quad (7b)$$

to be integrated between  $\xi = 0$  and  $\xi = 1$ , by imposing the sum rule given by Eq. 2, up to a finite upper size  $i_{\max}$ .

However, it is well known that ion bombardment also produces different kind of defects that may instead enhance the crystallization process. As an example, ion irradiation of an amorphous layer induces the nucleation and growth of crystalline silicon at temperature above 350 °C [17,18, 19, 20]. These defects (e.g. dangling-bonds like) are characterized by longer lifetimes, in the order of seconds at 250 °C and of 3 days at room temperature [21,22]. These circumstances strongly suggest that also long-living defects must be considered when modeling both amorphization and crystallization processes.

We then assume that these defects, produced by each impinging ion at a certain concentration level  $c_0$ , interact with the atoms or bonds at the amorphous cluster surface converting them into crystalline atoms, i.e. re-crystallization of amorphous regions occurs. Since their mobility is thermally activated, at low temperatures their influence is negligible and then amorphization

prevails on crystallization. The instantaneous value of defect concentration,  $\bar{c}_0$ , at the arrival of the  $j$ -th ion, will be:

$$\bar{c}_0 = c_0 \left[ 1 - \frac{c_{t=(j-1)\tau_0}}{\rho} \right] + c_{t=(j-1)\tau_0} \quad (8)$$

where  $c_{t=(j-1)\tau_0}$  is the concentration level established at the time  $(j - 1)\tau_0$ , corresponding to the impinging of the previous  $j-1$  ions,  $\tau_0$  being the time interval between the arrival of two successive ions in the same region:

$$\tau_0 = \frac{1}{\phi \pi r_0^2} \quad (9)$$

$\phi$  being the ion irradiation dose rate and  $r_0$  being the radius of the collision cascade.

During  $\tau_0$ , immediately after the prompt stage and before the arrival of the successive ion, due to in-pair annihilation process [17], defect concentration decreases following the relationship:

$$\frac{dc}{dt} = -a\sigma^2 f c^2 \quad (10)$$

where  $\sigma^2$  is the cross section for defect annihilation,  $a$  the average atomic distance, and  $f$  is the thermally activated defect jump frequency. Eq. 10 does not take into account for the thermal background of defects since that contribution is negligible in the investigated temperature range, where amorphization prevails on crystallization. The solution of Eq. 10 is:



$$c = \frac{\bar{c}_0}{1 + \bar{c}_0 a \sigma^2 f [t - (j - 1) \tau_0]} \quad j = 1, 2, 3, \dots \quad (11)$$

Figure 1 shows the typical dependence of the concentration of long living defects  $c$ , as a function of the irradiation fluence. At low fluence values, defect concentration increases very rapidly since in-pair annihilation, occurring during  $\tau_0$ , is only weakly effective (lower left inset in Fig. 1). Increasing ion fluence, the defect concentration approaches values at which the annihilation, proportional to  $c^2$ , becomes particularly relevant (upper right inset in Fig. 1), and defect density reaches a steady-state value of the order of the silicon atomic density  $\rho = 5 \times 10^{22} \text{ cm}^{-3}$ .

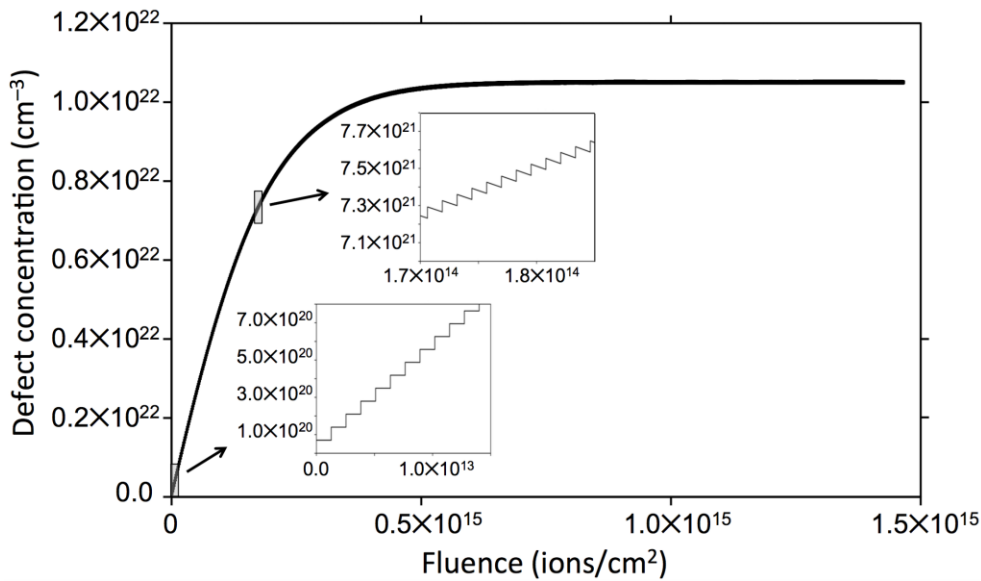


**Fig. 1.** Time dependence of the concentration of defects responsible for the re-crystallization of amorphous regions. The two insets show details on the evolution during the time interval among different collision cascades.

Analogously to the case of crystal grain nucleation, the stability of each amorphous cluster with  $i$  atoms is controlled by its free energy given by:

$$\Delta G_i = \Delta g_{ac}i + \sigma_{ac}O_i \quad (12)$$

where  $\Delta g_{ac}$  (positive for amorphous clusters) is the free energy change associated with the amorphization of a single atom, and  $\sigma_{ac}$  is the interface free energy of each atom at the amorphous–crystal interface. In the following, for simplicity, we have assumed a  $\Delta g_{ac}$  constant and independent of defect concentration on the surrounding crystal. Fine variations of  $\Delta g_{ac}$  as a function of the defect concentration cannot be excluded, but their effects on the ion–induced amorphization–crystallization process are beyond the aim of the present work. Irradiation increases the free energy not only of the crystalline region but also of the amorphous zones as evidenced by several experiments on the relaxation of amorphous silicon obtained by ion implantation [23, 24, 25]. The amorphous to crystal free energy increases with the irradiation fluence and decreases with the annealing temperature of the implanted layer. In any case the difference amounts to 10-20% of the value for the relaxed material [23].

Then, the amorphous cluster density will evolve through defect–mediated attachment or detachment of atoms at the amorphous–crystal interface, driven by the change of cluster free energy. This process occurs immediately at the end of the prompt stage of each collision cascade, and it lasts the time interval  $\tau_0$ . By using the reaction rate theory developed by Turnbull and Fisher [26], cluster growth or shrinkage is determined by two different atomic jump rates,  $k_i^+$  and  $k_i^-$ , given by:

$$k_i^+ = O_i c \Lambda f e^{-\frac{\Delta G_{i+1} - \Delta G_i}{2kT}} \quad (13a)$$

$$k_i^- = O_i c \Lambda f e^{\frac{\Delta G_{i+1} - \Delta G_i}{2kT}} \quad (13b)$$

where  $\Lambda$  is the volume transformed by each defect jump to the crystal or to the amorphous phase, and  $k$  the Boltzmann constant.

Hence, immediately after the prompt stage, amorphous clusters start to shrink since, in the amorphization regime, conversely to the case of crystal nucleation,  $\Delta G_i$  is a monotonic positive function of the cluster size, and  $k_i^-$  prevails on  $k_i^+$ . The shrinking velocity,  $k_i^- - k_i^+$ , strongly increases by decreasing cluster size as shown in Fig. 2. Small amorphous clusters are very unstable since, below a critical size, the average amorphization velocity can be lower than the crystallization one. The average amorphization growth rate,  $\langle k_i^\alpha \rangle$ , is given (for  $\chi_t \ll 1$ ) by:

$$\langle k_i^\alpha \rangle = O_i \frac{n_0}{\rho \tau_0} \quad (14)$$

The calculated values are also reported in Fig. 2 as dashed line. The two curves crosses at a critical size where the net average growth rate is equal to zero. This critical size is not constant during the transformation since the concentration of defects inducing re-crystallization increases with time.

Then, due to capillarity effects, the cluster density will evolve according to:

$$\frac{\partial N_{i,t}}{\partial t} = k_{i-1}^+ N_{i-1,t} + k_{i+1}^- N_{i+1,t} - (k_i^+ + k_i^-) N_{i,t} \quad i = 1, 2, 3, \dots, i_{\max} \quad (15a)$$

$$N_{0,t} = \rho - \sum_{i=1}^{i_{\max}} i N_{i,t} \quad (15b)$$

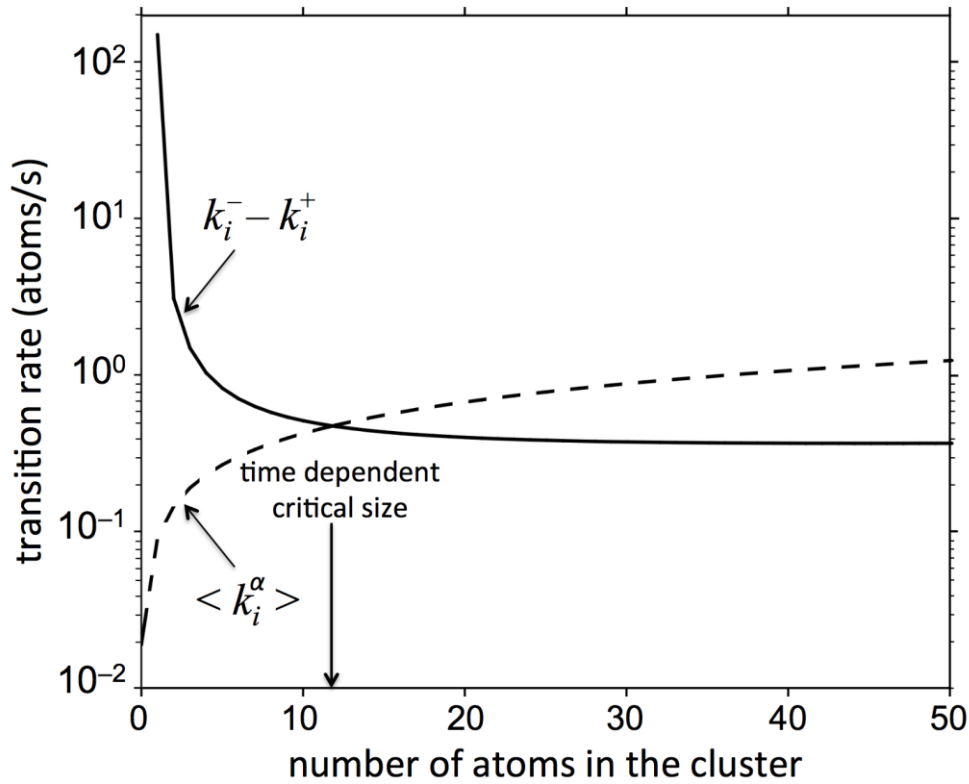


**Fig. 2.** Re-crystallization velocity,  $k_i^- - k_i^+$  (full line), and average amorphization growth rate,  $\langle k_i^\alpha \rangle$  (dashed line), as a function of cluster size, calculated using the following parameters:  $\Delta g_{ac} = 0.13$  eV,  $\sigma_{ac} = 0.14$  eV,  $c = 5 \times 10^{21}$  cm $^{-3}$ ,  $f = 1.1 \times 10^{-3}$  s $^{-1}$ ,  $\sigma^2 = 2 \times 10^{-14}$  cm $^3$ ,  $\Lambda = 2 \times 10^{-23}$  cm $^3$ ,  $n_0 = 8 \times 10^{20}$  cm $^3$ ,  $r_0 = 5$  nm,  $\phi = 1.5 \times 10^{12}$  cm $^{-2}$ s $^{-1}$ .

Numerical solutions of the coupled Eqs. 7a, 7b, 15a and 15b can be obtained following the method of Kelton *et al* [27]. Calculation starts with a relatively low value of  $i_{\max}$  ( $\sim 50$ ). Then  $i_{\max}$  is progressively increased to follow the growth of the amorphous clusters, with the constraints that the total number of atoms in clusters of size  $i_{\max}$  ( $i_{\max}N_{i_{\max},t}$ ) is negligible, i.e. several orders of magnitude lower than the silicon atomic density  $\rho$ . The final result of calculations is not affected by the particular choice of  $i_{\max}$  provided that:

$$i_{\max} N_{i_{\max}, t} < 10^{-13} \rho \quad (16)$$

Schematic of the model is shown in Fig. 3. At the prompt stage of the collision cascade amorphous clusters nucleate and grow (Fig. 3a), then long-living defects induce the cluster shrinkage (Fig. 3b). As a consequence, amorphous fraction abruptly increases at the prompt stage and then decreases in the time interval  $\tau_0$ , before the arrival of the successive ion, down to a level still higher than the one reached by the previous impinging ion (Fig. 3c).

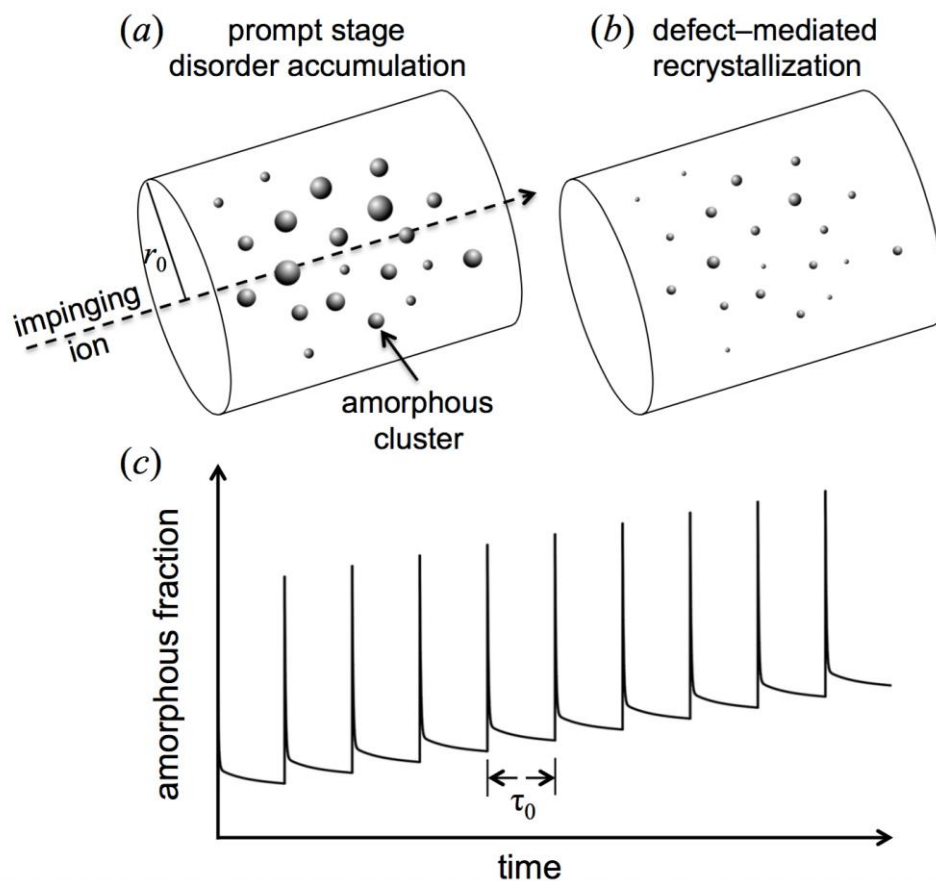


**Fig. 3.** Schematic picture of ion–beam amorphization in silicon. (a) The arrival of a single ion induces the nucleation and growth of amorphous cluster within the volume of its collision cascade; (b) in the time interval between the arrival of two successive ions on the same region, amorphous

clusters shrink; (c) amorphous fraction increases as a result of the balance between cluster nucleation/growth and defect-mediated re-crystallization.

It should be pointed out that the present description is consistent with the Jackson model describing the ion beam induced motion of a pre-existing amorphous-crystal planar interface [17]. Indeed, from Eqs. 2, 13a, and 13b, for temperatures at which crystallization prevails on amorphization, at large cluster sizes and for  $\chi_t = 0$  (planar interface), the average growth velocity approaches the value:

$$\frac{di}{dt} \sim O_i \left( c\Lambda f' - \frac{n_0}{\rho\tau_0} \right) \quad (17)$$

where  $f' = f[\exp(\Delta g_{ac}/2kT) - \exp(-\Delta g_{ac}/2kT)]$  since  $\Delta G_{i+1} - \Delta G_i$  approaches  $\Delta g_{ac}$  for  $i \rightarrow \infty$ .

By using the relationship  $i = \frac{4}{3}\pi R^3\rho$  between  $i$  and cluster radius  $R$ , Eq. 16 gives:

$$\frac{dR}{dt} = a \left( c\Lambda f' - \frac{n_0}{\rho\tau_0} \right) \quad (18)$$

and, in unit of ion fluence, we get the same functional form proposed by Jackson in his model [17]:

$$\frac{dR}{d\phi} = \frac{ac\Lambda f'}{\dot{\phi}} - V_\alpha \quad (19)$$

© 2019. This manuscript version is made available under the CC-BY-NC-ND 4.0 license  
<https://creativecommons.org/licenses/by-nc-nd/4.0/>

This is the postprint version of an article accepted for publication in Nuclear Instruments and Methods in Physics Research Section B: Beam Interactions with Materials and Atoms (Elsevier). The Version of Record is available online at  
<https://doi.org/10.1016/j.nimb.2019.11.009>

where  $V_\alpha = a\pi r_0^2 n_0/\rho$  is the amorphous volume created at the crystal–amorphous interface at the arrival of each ion on the area  $\pi r_0^2$ .

### 3. Results and discussion

#### 3.1 Amorphization at cryogenic temperature

Let's start to examine silicon amorphization at cryogenic temperatures (in the range 50–100K), where long-living defect mobility is negligible. Indeed, jump rate  $f$  is thermally activated:

$$f = f_0 \exp\left(-\frac{E_a}{kT}\right) \quad (20)$$

with activation energy,  $E_a$ , of about 1 eV, and pre-exponential factor  $f_0$  [17, 18, 19]. Under these conditions, amorphization proceeds only by cluster nucleation and growth occurring during the prompt stage of each collision cascade, described by Eqs. 7a and 7b.

Fig. 4 shows the fit of the present model (full line) to the experimental data reporting the silicon amorphous fraction as a function of ion fluence for irradiation with 380 keV Sn (open squares) or 380 keV Si (open circles), at a substrate temperature of 90 K, taken from Ref. [28]. At these temperatures defect mobility is negligible, the amorphous fraction as a function of fluence, described by Eqs. 1a and 1b, depends only on the product  $n_0\pi r_0^2$ , i.e. on the number of atoms converted in the amorphous state by the single ion per unit length during the prompt stage of the collision cascade. This value should be compared with the number of displaced atoms per unit length,  $n_1$ , given by the Monte Carlo simulation code TRIM [29]. We find that the best fit for the simulation requires values of  $n_0\pi r_0^2$  of  $3.4 \times 10^9 \text{ cm}^{-1}$  for the irradiation with 380 keV Sn, and  $5.2 \times 10^8 \text{ cm}^{-1}$  for the irradiation with 380 keV Si respectively, both higher than  $n_1$  by a factor in the range 6–8 (Tab. II). This behavior was already observed in the case of IBIEC [17], or in the regime



of ion-beam-induced crystal grain nucleation of amorphous silicon [18, 19], and it is in agreement with numerical simulation of the amorphization efficiency according to which the crystal to amorphous transition occurs when an amount of self interstitials defects greater than 13–15% is inserted in the host lattice [30].

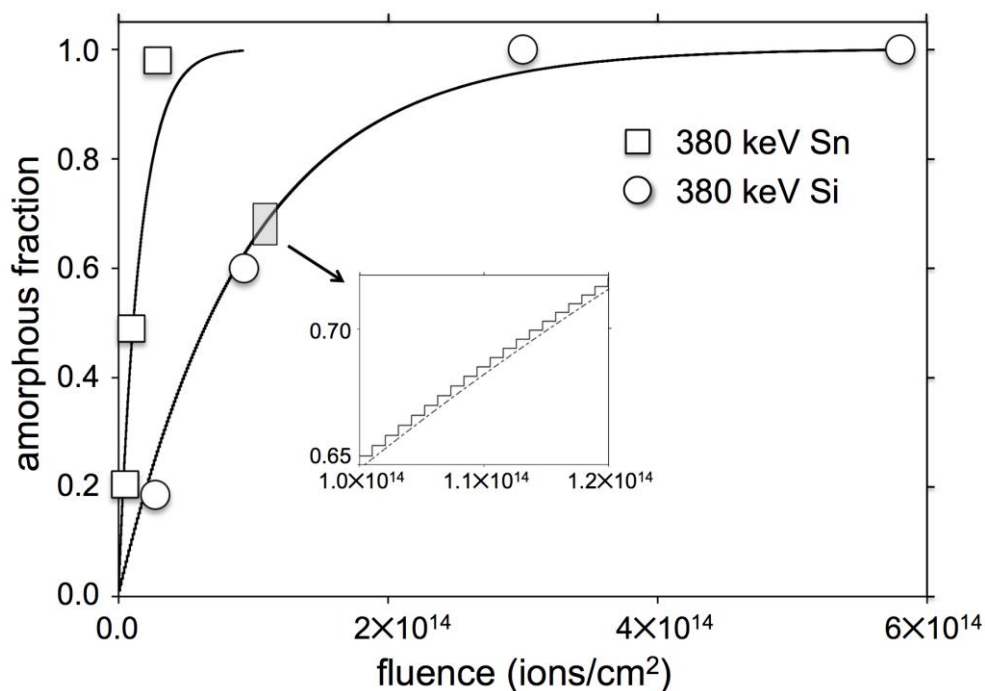


**Fig. 4.** Amorphous fraction as a function of the ion fluence for silicon irradiated with 380 keV Sn ions (□) or 380 keV Si ions (○) at a temperature of 90 K. Solid lines are the fits to the data from Ref. 15 using the model described in the text. Details of the time evolution among successive collision cascades are shown in the inset where dashed line is calculated by using Eqs. 21 and 22.

Inset in Fig. 4 is a detail of the fitting curve (full line) for a time interval containing only few collision cascades. What it is seen as a continuous trend, it is actually the result of a discontinuous sequence of an abrupt increase of the amorphous fraction at the prompt stage of each collision

cascade. It should be pointed out that the average behavior of the amorphous fraction versus ion fluence as described by Eqs. 1a and 1b, exhibits the same dependence as predicted by the Avrami–Johnson–Mehl equation [31-34]:

$$\frac{d\chi}{d\phi} = \frac{1 - \chi}{\phi_a} \quad (21)$$

where  $\chi$  is the amorphous fraction as a function of irradiation fluence  $\phi$ , i.e.:

$$\chi = 1 - \exp\left(-\frac{\phi}{\phi_a}\right) \quad (22)$$

where:

$$\phi_a = \frac{\rho}{\pi r_0^2 n_0} \quad (23)$$

Eq. 22 describes an amorphization process that proceeds through progressive accumulation of isolated amorphous atoms (dashed line in the inset of Fig. 4), at an average time rate of  $n_0/\rho\tau_0$ , rather than by nucleation and growth of amorphous clusters. Then, at liquid nitrogen temperature, since the defects responsible for re-crystallization are immobile, the Avrami–Johnson–Mehl (AJM) description based on Eq. 21 and the one based on nucleation and growth of clusters according to Eqs. 7a and 7b, are perfectly equivalent. We also point out that the functional form given by Eq. 22 coincides with the theoretical expression proposed by Gibbons [15] (involving overlap of damage pockets) for the case  $m = 0$  ( $m$  being the minimum number of overlaps in the same region necessary to produce amorphization) with a damaged area produced by a single ion track right equal to  $\pi r_0^2 n_0/\rho$ , i.e. the reciprocal of  $\phi_a$ .

### 3.2 Amorphization above cryogenic temperatures

The description based on nucleation and growth of amorphous clusters, and particularly their stability as a function of size, becomes relevant at higher irradiation temperatures, where the competition with re-crystallization is significant due to the increase of defect mobility. As an example, the experimental data (Ref. 35) for irradiation of single crystal silicon wafers with 1 MeV Ge<sup>+</sup> ions at a substrate temperature of 373 K (open circles), with 400 keV Ge<sup>+</sup> ions at a substrate temperature of 373 K (open squares), or at a room temperature (open diamonds), respectively, at a dose rate of  $1.5 \times 10^{12} \text{ cm}^{-2} \text{ s}^{-1}$  are shown in Fig. 5.

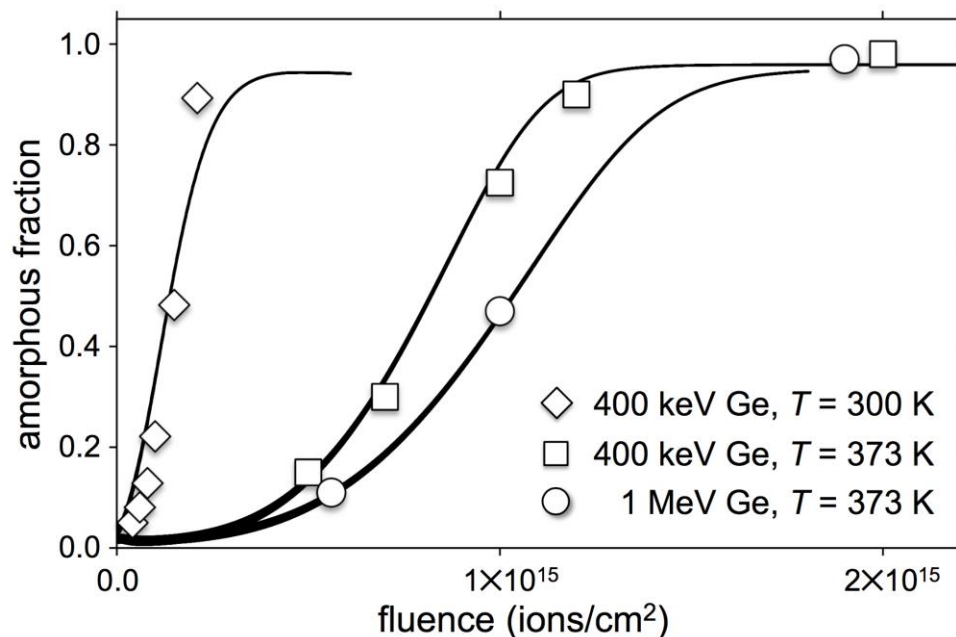


**Fig. 5.** Amorphous fraction as a function of the ion fluence for silicon irradiated with 400 keV Ge ions at substrate temperatures of 300 K ( $\diamond$ ) or 373 K ( $\square$ ), or irradiated with 1 MeV Ge ions at 373 K ( $\circ$ ) from Ref. [35]. For all the experiments the irradiation dose rate was fixed to  $1.5 \times 10^{12} \text{ cm}^{-2} \text{ s}^{-1}$ . Solid lines are fits to the data using the present model.

Compared with the irradiation data at 90 K (Fig. 4), the amorphization kinetics at room temperature or above is significantly slower. This indicates clearly that the growth of amorphous clusters is contrasted by their shrinking due to the presence of mobile defects responsible for re-crystallization. We also observe that the increase of the amorphous fraction as a function of ion fluence follows a trend different from that observed at 90 K. At cryogenic temperature (Fig.4) a monotonic negative concavity is revealed, whilst at room temperature, or above, the fluence dependence is more complex showing an inflection point, i.e. a change in the sign of the concavity. To fit such experimental data (Fig. 5) Campisano et al. [35] used an AJM expression of the kind:

$$\chi = 1 - \exp \left[ - \left( \frac{\phi}{\phi_a} \right)^n \right] \quad (24)$$

with  $n = 3.5$ . According to our model, however, at relatively high temperatures amorphization proceeds slowly, and an incubation time, before stable amorphous clusters form, characterizes the transformation. The concentration of defects responsible for re-crystallization is far from its steady-state value for a significant extent of the transformation (see Fig. 1 as an example). Then, the Avrami–Johnson–Mehl description cannot be used since nucleation rate and growth velocity of the amorphous clusters are not constant during the irradiation time. Continuous lines in Fig. 5 are fits of our model to the data, by using the parameter values shown in Tab. I.

Tab. I Parameter values used to fit the experimental data from Ref. [35] shown in Fig. 5 according to the theoretical model described in the text.

ion irradiation	$\dot{\phi}$ (cm <sup>-2</sup> s <sup>-1</sup> )	$T$ (K)	$\Delta g_{ac}$ (eV)	$\sigma_{ac}$ (eV)	$n_0$ (cm <sup>-3</sup> )	$r_0$ (nm)	$c_0$ (cm <sup>-3</sup> )	$\sigma^2$ (cm <sup>-2</sup> )	$\Lambda$ (cm <sup>3</sup> )	$f$ (s <sup>-1</sup> )
400 keV Ge	1.5x10 <sup>12</sup>	300 K	0.13	0.14	8.0x10 <sup>20</sup>	5.6	1.05x10 <sup>20</sup>	2x10 <sup>-14</sup>	2x10 <sup>-23</sup>	1.6x10 <sup>-5</sup>
400 keV Ge	1.5x10 <sup>12</sup>	373 K	0.13	0.14	8.0x10 <sup>20</sup>	5.6	1.05x10 <sup>20</sup>	2x10 <sup>-14</sup>	2x10 <sup>-23</sup>	1.1x10 <sup>-3</sup>
1 MeV Ge	1.5x10 <sup>12</sup>	373 K	0.13	0.14	7.1x10 <sup>20</sup>	5.0	6x10 <sup>19</sup>	2x10 <sup>-14</sup>	2x10 <sup>-23</sup>	1.1x10 <sup>-3</sup>

We have assumed that thermodynamic parameters,  $\Delta g_{ac}$  and  $\sigma_{ac}$ , defect annihilation cross section,  $\sigma^2$ , and volume crystallized by each defect jump,  $\Lambda$ , do not change by varying temperature and the defect concentration in the surrounding crystal. We have also assumed that each defect jump at the cluster surface induces the transition of one atom from the amorphous to the crystalline phase, i.e.  $\Lambda = 1/\rho = 2 \times 10^{-23} \text{ cm}^3$ . Instead, defect jump frequency,  $f$ , was adapted according to the two temperatures used in the experiments (300 and 373 K). The concentrations of atoms converted from the crystal to the amorphous phase,  $n_0$ , of the defects responsible for re-crystallization,  $c_0$ , and the radius,  $r_0$ , of the collision cascade were allowed to change for the two different ion irradiation energies. In a similar investigation [36] using different ion masses, fluences and target temperatures the experimental data were described in terms of a two-stage nucleation-limited amorphization process. Initially the process is limited by the availability of nucleation sites and then by the supply of simple defects to these clusters. Our model describes simultaneously amorphous growth and shrinkage.

A relevant achievement of the present description is its capability to describe the amorphization process for a wide range of ion energy and ion mass, spanning from heavy to light ions. As an example Fig. 6 shows, as solid lines, the fits to the experimental data for irradiation with Sn, Si, or C ions at an incident energy of 380 keV and substrate temperatures of 90 or 300 K [28].

The fitting parameter values are listed in Tab. II. The model accounts for the details of the damage accumulation kinetics either in extremely dilute (380 keV C) or dense collision cascade (380 keV Sn). We notice, again, that the trend of the amorphous fraction dependence on the fluence changes by increasing temperature as evidenced by the different slopes, in the semi-logarithmic plot, of the curves fitting the data at 90 and 300 K, respectively. At cryogenic temperature the transformation proceeds by the accumulation of amorphous clusters of small sizes, and the trend of the amorphous fraction versus fluence mimics the one described by the AJM equation with exponent 1. At higher temperature, amorphous clusters of small sizes are unstable. Only those exceeding a critical size, fluence dependent, can grow by trapping most of the  $n_0$  atoms converted in the amorphous state by each impinging ion per unit volume, and leading to a AJM-like behavior with exponent larger than 1.

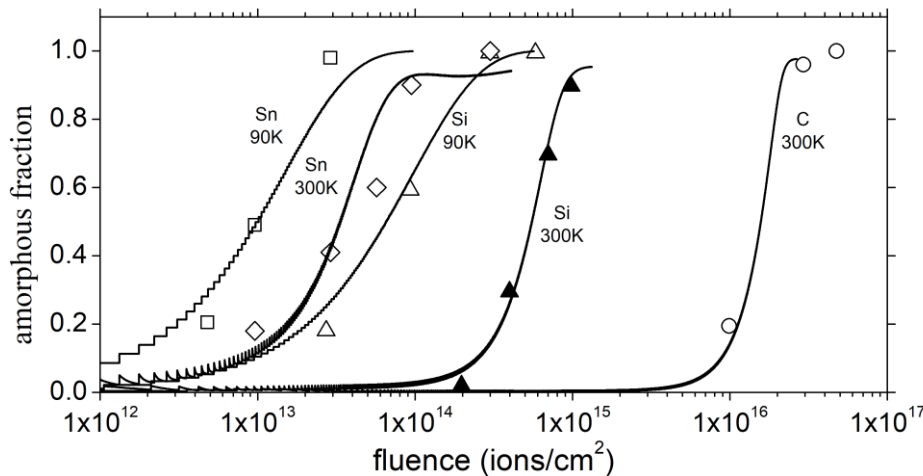


**Fig. 6.** Amorphous fraction as a function of the ion fluence for irradiation at an energy of 380 keV with various ions, C, Si, and Sn, at either room temperature or 90 K from Ref. [28]. Calculated curves are also plotted (solid lines).

Tab. II Parameter values used to fit the experimental data from Ref. [28] shown in Fig. 6

according to the model described in the text.

ion	$\dot{\phi}$	$T$	$\Delta g_{ac}$	$\sigma_{ac}$	$n_0$	$r_0$	$c_0$	$\sigma^2$	$\Lambda$	$f$
irradiation	( $\text{cm}^{-2}\text{s}^{-1}$ )	(K)	(eV)	(eV)	( $\text{cm}^{-3}$ )	(nm)	( $\text{cm}^{-3}$ )	( $\text{cm}^{-2}$ )	( $\text{cm}^3$ )	( $\text{s}^{-1}$ )
380 keV Sn	$3 \times 10^{11}$	90	0.13	0.14	$1.5 \times 10^{21}$	8.5	$2.2 \times 10^{20}$	$2 \times 10^{-14}$	$2 \times 10^{-23}$	$\sim 0$
380 keV Si	$3 \times 10^{11}$	90	0.13	0.14	$5.5 \times 10^{20}$	5.5	$7.2 \times 10^{19}$	$2 \times 10^{-14}$	$2 \times 10^{-23}$	$\sim 0$
380 keV Sn	$3 \times 10^{11}$	300	0.13	0.14	$1.5 \times 10^{21}$	8.5	$2.2 \times 10^{20}$	$2 \times 10^{-14}$	$2 \times 10^{-23}$	$1.6 \times 10^{-5}$
380 keV Si	$3 \times 10^{11}$	300	0.13	0.14	$5.5 \times 10^{20}$	5.5	$7.2 \times 10^{19}$	$2 \times 10^{-14}$	$2 \times 10^{-23}$	$1.6 \times 10^{-5}$
380 keV C	$3 \times 10^{11}$	300	0.13	0.14	$2.0 \times 10^{20}$	3.0	$7.0 \times 10^{18}$	$2 \times 10^{-14}$	$2 \times 10^{-23}$	$1.6 \times 10^{-5}$

The agreement of the experimental data with simulations evidences the effectiveness of the model in taking into account for the incubation fluence, i.e. the ion fluence necessary to build up a sufficiently large population of stable amorphous clusters, a characteristic feature of a nucleation–limited phase transition. The incubation fluence increases by decreasing the ion mass ( $2 \times 10^{13} \text{ cm}^{-2}$  for Sn,  $3 \times 10^{14} \text{ cm}^{-2}$  for Si, and  $1 \times 10^{16} \text{ cm}^{-2}$  for C), a behavior that is clearly reproduced by the simulations.

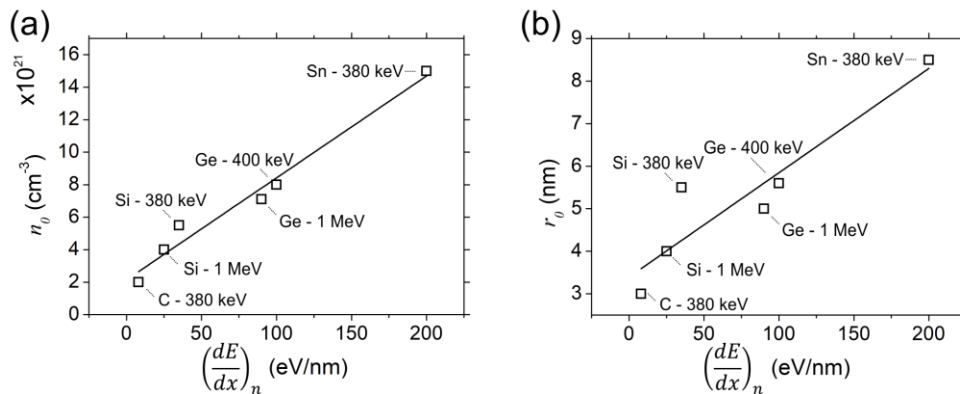


**Fig. 7.** (a) Concentration  $n_0$  of atoms converted into the amorphous state and (b) radius of the collision cascade  $r_0$  as a function of the nuclear stopping power for irradiation at several energies and with various ions, C, Si, Ge and Sn. Solid lines are linear fits to the data points.

As shown in Fig. 7,  $n_0$  and  $r_0$  scale with the maximum of the nuclear stopping power, as calculated by TRIM [29], ranging from  $2 \times 10^{20} \text{ cm}^{-3}$  and 3 nm for 380 keV C (8 eV/nm) to  $1.5 \times 10^{21} \text{ cm}^{-3}$  and 8.5 nm for 380 keV Sn (200 eV/nm). This behavior is quite expected for  $n_0$ , since, according to the modified Kinchin-Pease equation [see for details ref. 37]:

$$N_d = 0.8 \left( \frac{dE}{dx} \right)_n \cdot \frac{1}{2E_d} \cdot \phi \quad (25)$$

Where  $N_d \sim n_0$  is the number of displacement per unit volume,  $\left( \frac{dE}{dx} \right)_n$  is the nuclear stopping power and  $E_d = 15 \text{ eV}$  is the displacement energy for Si.

Deviations from the linear trend (e.g.  $r_0$  value for 380 keV Si) could be relied on the heterogeneities of the data employed for the fits, collected in several laboratories by means of different experimental techniques.

### 3.3 Dose–rate dependence

Amorphization under conditions where dynamic re–crystallization is extremely significant depends not only on the substrate temperature but also on irradiation dose rate. Fig. 8 reports the damage yield in silicon irradiated with 1 MeV Si ions at a fixed fluence of  $1 \times 10^{15} \text{ cm}^{-2}$  as a function of the substrate temperature and for three different dose rates:  $2.88 \times 10^{11} \text{ cm}^{-2} \text{ s}^{-1}$  (open circles),



$3.57 \times 10^{12} \text{ cm}^{-2} \text{ s}^{-1}$  (full circles), and  $2.63 \times 10^{13} \text{ cm}^{-2} \text{ s}^{-1}$  (open squares) [38]. Continuous lines are calculations using the parameter values reported in Tab. III. It should be noted that a unique set of parameters reproduces the process dynamics as a function of dose rate, in a wide temperature range, extending from values where amorphization is inhibited to temperatures at which full amorphization occurs.

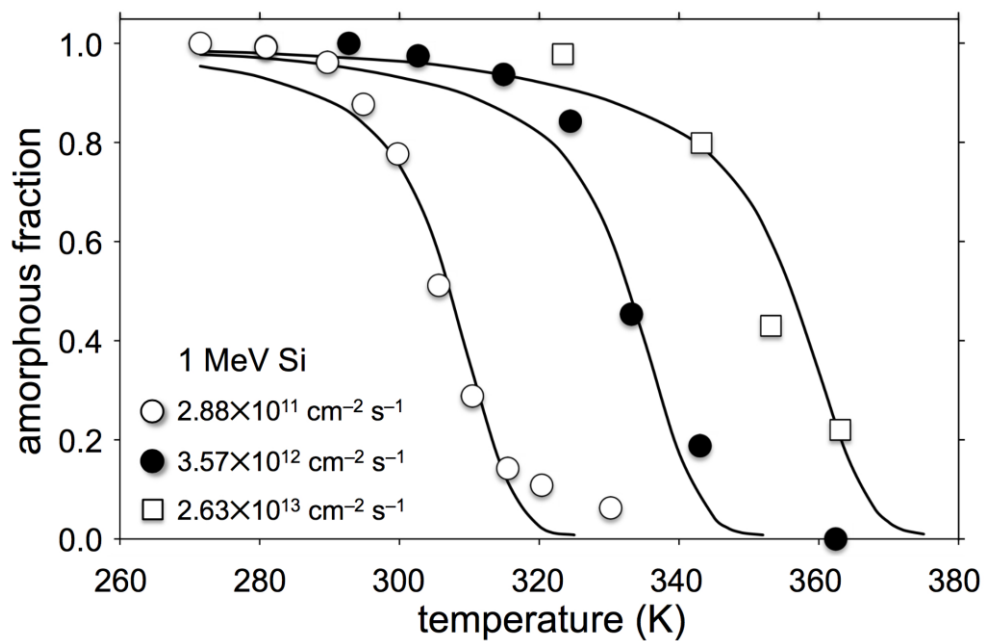


**Fig. 8.** Amorphous fraction in a single crystal silicon irradiated with 1 MeV Si ions to a fluence of  $1 \times 10^{15} \text{ cm}^{-2}$  as a function of the substrate temperature and for dose rates of  $2.88 \times 10^{11} \text{ cm}^{-2} \text{ s}^{-1}$  (open circles),  $3.57 \times 10^{12} \text{ cm}^{-2} \text{ s}^{-1}$  (closed circles),  $2.63 \times 10^{13} \text{ cm}^{-2} \text{ s}^{-1}$  (open squares), respectively, from Ref. [38]. Solid lines are fits to the data.

Tab. III Parameter values used to fit the experimental data from Ref. [38] shown in Fig. 8 according to the theoretical model described in the text.

ion irradiation	$\Delta g_{ac}$ (eV)	$\sigma_{ac}$ (eV)	$n_0$ (cm <sup>-3</sup> )	$r_0$ (nm)	$c_0$ (cm <sup>-3</sup> )	$\sigma^2$ (cm <sup>-2</sup> )	$\Lambda$ (cm <sup>3</sup> )	$f_0$ (s <sup>-1</sup> )	$E_a$ (eV)
1 MeV Si	0.13	0.14	$4 \times 10^{20}$	4	$6.0 \times 10^{19}$	$2 \times 10^{-14}$	$2 \times 10^{-23}$	$4 \times 10^{12}$	1.1

Our treatment successfully extends the phenomenological model developed by Jackson for the ion beam induced motion of a pre-existing amorphous-crystal silicon planar interface, to the amorphous nucleation and growth in irradiated single crystal silicon. To take into account for the effect of temperature in the amorphization process we introduced, in the simulation, the thermally activated dependence of the defect jump frequency  $f(T)$  as a fit parameter. All the data (Fig. 8) are described, by a unique activation energy  $E_a = 1.1$  eV and a pre-exponential factor  $f_0 = 4 \times 10^{12}$  s<sup>-1</sup>.

The values of jump frequency,  $f$ , as obtained by the fits to all the experimental data presented so far, are shown in Fig. 9 in a semi-logarithmic plot as a function of the reciprocal temperature. For the 1 MeV Si irradiation we have plotted the jump frequency values (diamonds) corresponding to substrate temperatures where the amorphous fraction reaches 50%. This procedure has been performed for the three different dose rates shown in Fig. 8. We report as guide lines two solid lines describing the activation energy ranges, corresponding with a slope of 0.6 and 1.1 eV, respectively.

It must be remarked that the investigated temperature range spans less than 100 degrees. The experimental uncertainty and the comparison of data acquired in several laboratories with different experimental setups justify the corresponding large variation in the estimated activation energy for defect migration and in the pre-exponential factor.

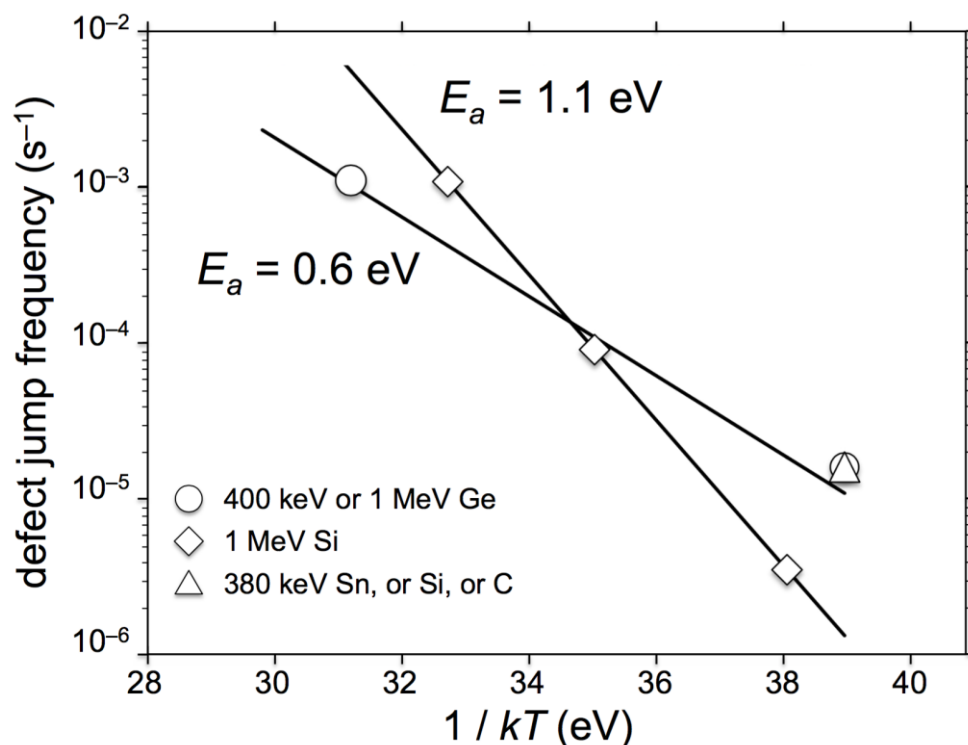


**Fig. 9.** Defect jump frequency adopted to fit the experimental data as a function of the reciprocal temperature. The reported jump frequencies are the values obtained by the fit of the data of Fig. 5 (open circles), Fig. 6 (open triangle), and Fig. 8 (open diamond). The two solid lines corresponding to 0.6 and 1.1 eV respectively are guidelines for the activation energy range.

This activation energy is significantly lower than the value characterizing the kinetics of the reverse transformation ( $E_a = 1.36$  eV), i.e. the spontaneous nucleation and growth of crystal grains in an amorphous silicon layer under ion beam irradiation at higher temperatures [18, 19]. It should be considered, however, that the two processes (amorphous or crystal nucleation) occur at quite different temperature ranges: below 200 °C the former, well above 350 °C the latter. Indeed, studies on the annealing kinetics of defects in amorphous silicon have shown that a whole variety of defect structures may exist with a large spectrum of energies ranging between 0.3 and 2.7 eV [23, 39, 40,

41]. The larger range in the low values characterizes the annealing of isolated amorphous zone. The 2.7 eV value is associated to the epitaxial re-growth of a planar amorphous-crystal interface. The irregularity of the interface of any nanometer sized zone and the local atomic arrangement at the surface may be responsible for the wide range of activation energies. Therefore, it should not surprise that defects promoting damage recovering at temperatures where amorphization prevails on crystallization can be different from the ones responsible for crystallization at higher temperatures, where the transformation proceeds in the opposite direction (amorphous to crystal). In our description, we have considered, for simplicity, the existence of a single type of defects responsible for the damage recovering, characterized, in the investigated temperature range, by a single activation energy for migration. The actual situation is, of course, more complicated: a lot of defects are present; each of them is governed by a characteristic energy for migration. At low temperature defects with low activation energy are mobile, at high temperature these defects have already disappeared and remain those with a high energy for migration. In ref. 8 using pulsed ion beam irradiation two activation energies of 0.073 and 0.42 eV were determined below and above 60°C respectively for the migration of interstitial and vacancy.

Our model also predicts the structural characteristic of the damage resulting from the balance between prompt amorphization and re-crystallization, at a given value of the amorphous fraction. This effect is shown in Fig. 10 where the calculated cluster size distributions is plotted in a semi-logarithmic scale, for 1 MeV Ge<sup>+</sup> irradiation of silicon at 373 K, at two different dose rates,  $3.0 \times 10^{12} \text{ cm}^{-2} \text{ s}^{-1}$  and  $1.5 \times 10^{12} \text{ cm}^{-2} \text{ s}^{-1}$  respectively, and for 380 keV C<sup>+</sup> irradiation at 300 K at a dose rate of  $3.0 \times 10^{11} \text{ cm}^{-2} \text{ s}^{-1}$ . For all the irradiation conditions, calculations were carried out up to ion fluences corresponding to an amorphous volume fraction equal to 40%. The parameters were set to the values reported in Tab. II.

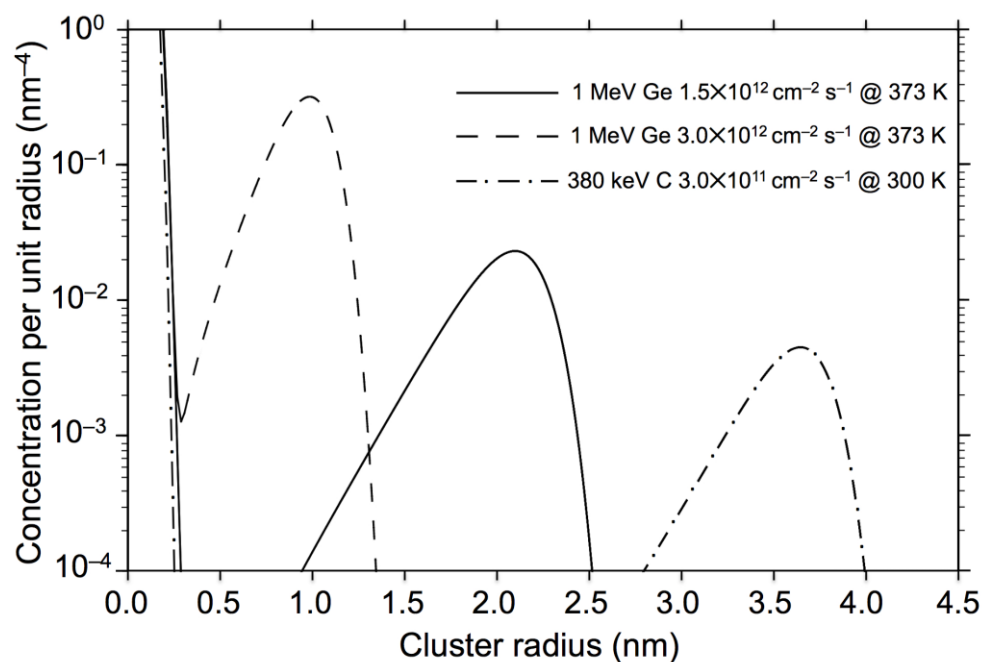


**Fig. 10.** Calculated size distributions of amorphous clusters in undoped silicon irradiated with 1 MeV Ge ions at two different dose rates,  $1.5 \times 10^{12} \text{ cm}^{-2} \text{ s}^{-1}$  (full line) and  $3.0 \times 10^{12} \text{ cm}^{-2} \text{ s}^{-1}$  (dashed line) and with 380 keV C ions at the dose rate of  $3.0 \times 10^{11} \text{ cm}^{-2} \text{ s}^{-1}$  (dot-dashed line) respectively. The adopted fluences produce the 40% amorphous phase.

For irradiation with 1 MeV Ge<sup>+</sup> at 373 K the peak of cluster size distribution shifts from 1 nm (dashed line) to about 2 nm (full line), by decreasing the dose rate from  $3.0 \times 10^{12} \text{ cm}^{-2} \text{ s}^{-1}$  to  $1.5 \times 10^{12} \text{ cm}^{-2} \text{ s}^{-1}$ . In the case of 380 keV C<sup>+</sup> irradiation at 300 K, the same amorphization fraction is associated with cluster size distribution peaked at even larger radius, about 3.5 nm (dot-dashed line).

### 3.4 Doping effects

Ion beam induced crystallization (IBIEC) enhancement due to the presence of dopant atoms is a pretty known effect [42]. It was extensively investigated and interpreted by assuming that defects

promoting the amorphous to crystal phase transition are allowed to exist in charge states and their concentration,  $c_0$ , in doped silicon increases with respect to undoped material. In the already mentioned paper, Campisano *et al.* [35] have analyzed the influence of doping, with boron or arsenic, on the time dependence of the amorphous fraction under irradiation with 1 MeV Ge<sup>+</sup> ions at a substrate temperature of 100 °C and dose rate of  $1.5 \times 10^{12} \text{ cm}^{-2} \text{ s}^{-1}$ . The corresponding experimental data are shown in Fig. 11 where the amorphous fraction is plotted as a function of the fluence for undoped (open squares), As-doped (full triangles,  $5 \times 10^{12} \text{ As/cm}^{-3}$ ), or B-doped (full circles,  $10^{20} \text{ B/cm}^3$ ) silicon wafer. All the fitting parameters are summarized in Tab. IV.

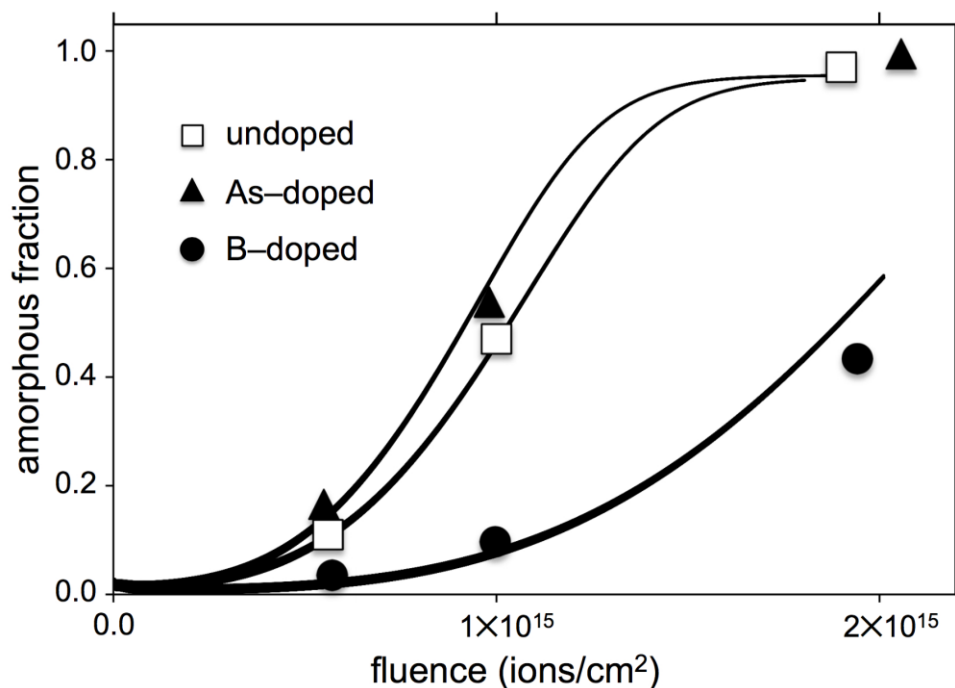


**Fig. 11.** Amorphous fraction as a function of the ion fluence for undoped (□), As-doped (▲), and B-doped (●) silicon samples irradiated with 1 MeV Ge ions at a substrate temperature of 100 °C from Ref. [35]. Solid lines are a fit to the data by the present model.

Tab. IV Parameter values used to fit the experimental data from Ref. [35] shown in Fig. 11

according to the theoretical model described in the text.

ion irradiation	$\dot{\phi}$ ( $\text{cm}^{-2}\text{s}^{-1}$ )	$T$ (K)	Dopin g	$\Delta g_{ac}$ (eV)	$\sigma_{ac}$ (eV)	$n_0$ ( $\text{cm}^{-3}$ )	$r_0$ (nm)	$c_0$ ( $\text{cm}^{-3}$ )	$\sigma^2$ ( $\text{cm}^{-2}$ )	$\Lambda$ ( $\text{cm}^3$ )	$f$ ( $\text{s}^{-1}$ )
1 MeV Ge	$1.5 \times 10^{12}$	373	–	0.13	0.14	$7.1 \times 10^{20}$	5	$6.0 \times 10^{19}$	$2 \times 10^{-14}$	$2 \times 10^{-23}$	$1.1 \times 10^{-3}$
1 MeV Ge	$1.5 \times 10^{12}$	373	B	0.13	0.14	$7.1 \times 10^{20}$	5	$8.5 \times 10^{19}$	$2 \times 10^{-14}$	$2 \times 10^{-23}$	$1.1 \times 10^{-3}$
1 MeV Ge	$1.5 \times 10^{12}$	373	As	0.11	0.14	$7.1 \times 10^{20}$	5	$8.0 \times 10^{19}$	$2 \times 10^{-14}$	$2 \times 10^{-23}$	$1.1 \times 10^{-3}$

The present theoretical description explains the difference in the amorphization kinetics between undoped and B-doped sample, by adjusting only the parameter  $c_0$ , i.e. the concentration of mobile defects generated at the arrival of each single ion. In particular  $c_0$  have to be increased in the case of B-doped sample ( $c_0$  changes from  $6 \times 10^{19} \text{ cm}^{-3}$  for the undoped sample to  $8.5 \times 10^{19} \text{ cm}^{-3}$  for the B-doped one).

The effect of As may seem somewhat surprising as it is known that this dopant, like B, enhances ion beam induced crystallization at planar amorphous–crystal interfaces. However, within the context of the present description, where kinetics effects are combined to thermodynamic argument (through the capillarity theory), it should be noted that the presence of arsenic decreases the free energy difference  $\Delta g_{ac}$  between the amorphous and crystal phase, an effect that has been already observed during the pure thermal crystallization regime [43]. The reduction of  $\Delta g_{ac}$  makes the amorphous clusters more stable and counterbalances the re-crystallization enhancement associated with the increase of  $c_0$ . The fit to the As data shown in Fig. 11 was obtained still by increasing  $c_0$ , to the value of  $8 \times 10^{19} \text{ cm}^{-3}$ , in order to take into account for the kinetics enhancement of re-crystallization induced by arsenic, and, at the same time, by diminishing  $\Delta g_{ac}$  to the value of

0.11 eV, coherently to what was observed from the investigation of the crystal grain nucleation in As-doped amorphous silicon [43].

#### **4. Conclusions**

We have shown that the amorphization kinetics in ion beam irradiated crystal silicon can be described within the framework of the nucleation and growth theory. Nucleation and growth of amorphous clusters occurs during time regime of collisional cascade processes ( $10^{-12}$  s). Cluster stability depends on their free energy content, and their growth is contrasted by the action of long-living defects, also generated by the ion beam, whose concentration keeps far from its steady-state value for a significant extent of the transformation. As a consequence nucleation rate and growth velocity remain transient, even after the incubation fluence, i.e. the ion dose necessary to form a suitable high concentration of clusters at sizes where the amorphization growth rate overcomes the re-crystallization one. The model mirrors and extends the theoretical descriptions already proposed to interpret the layer-by-layer amorphization and recrystallization occurring at planar amorphous-single crystal interface and the ion-beam assisted nucleation and growth of crystalline clusters in the amorphous silicon material. It explains all the peculiar features of the ion-beam induced silicon amorphization process (transient behavior, dependence on temperature and on irradiation parameters in a wide range of ion energy and mass), including effects associated with the presence of doping. Model predictions are in very good agreement with experiments, taking into account the heterogeneities of the data employed, collected in several laboratories by means of different experimental techniques.

#### **Acknowledgements**



© 2019. This manuscript version is made available under the CC-BY-NC-ND 4.0 license  
<https://creativecommons.org/licenses/by-nc-nd/4.0/>

This is the postprint version of an article accepted for publication in Nuclear Instruments and Methods in Physics Research Section B: Beam Interactions with Materials and Atoms (Elsevier). The Version of Record is available online at  
<https://doi.org/10.1016/j.nimb.2019.11.009>

The authors acknowledge Nanoscience Foundry and Fine Analysis (NFFA-MIUR Italy Progetti Internazionali) and DSFTM-CNR for providing financial support.

## References

- [1] E. Rimini, Ion Implantation: basics to device fabrication, Kluwer, Boston, 1995.
- [2] J. -Y. Jin, J. Liu, U. Jeong, S. Metha, and K. Jones J. Vac. Sci. Technol. B 20 (2002) 422.
- [3] J. E. E. Baglin, H. B. Harrison, J. L. Tandom and J. S. Williams, in: J. S. Williams and J. M. Poate (Eds.), Ion Implantation and Beam Processing, Chapter 11, Academic Press, 1984.
- [4] A. Alberti, A. La Magna, M. Cuscunà, G. Fortunato, , and V. Privitera, Appl. Phys. Lett. 96 (2010) 142113.
- [5] L. Pelaz, L.A. Marqués, J. Barbolla, J. Appl. Phys. 96 (2004) 5947-5976.
- [6] E. Wendler, Nucl. Instrum. Methods Phys. Res. B 267 (2009) 2680.
- [7] W. Wesch, E. Wendler, C.S. Schnohr, Nucl. Instrum. Methods Phys. Res. B 277 (2012) 58.
- [8] J. B. Wallace, L. B. Bayu Aji, A. A. Martin, S. J. Shin, L. Shao, S. O. Kucheyev, Sci Rep. 7 (2017) 39754.
- [9] J. B. Wallace, S. Charnvanichborikarn, L. B. Bayu Aji, M. T. Myers, L. Shao, S. O. Kucheyev, J. Appl. Phys. 118 (2015) 135709.
- [10] a) E. Wendler, Nucl. Instrum. Methods Phys. Res. B 267 (2009) 2680.  
b) E. Wendler, W. Wesh, in: B. Kramer (Ed.), Advanced in Solid State Physics, Vol. 44, Springer-Verlag. Heidelberg, 2004, pp363-374.
- [11] K. Trachenko, J. M. Pruneda, E. Artacho and M. T. Dove , Phys. Rev B 71 (2005) 184104.
- [12] F. L. Vook in: J. E. Whitehouse (Ed.), Radiation Damage and Defects in Semiconductors, Inst. Phys. Conf. Ser. No. 16, Institute of Physics, London, 1973, p. 60.
- [13] J. R. Dennis, E. B. Hale, J. Appl. Phys. 49 (1978) 1119-1127.

- [14] F.F. Morehead, B.L. Crowder, Radiat. Eff. 6 (1970) 27-32.
- [15] J.F. Gibbons, Proc. IEEE 60 (1972) 1062-1096.
- [16] L. Pelaz, L. A. Marques, M. Aboy, J. Barbolla, Nucl. Instr. Meth. B 216 (2004) 41-45.
- [17] K.A. Jackson, J. Mater. Res. 3 (1988) 1218-1226.
- [18] C. Spinella, S. Lombardo, F. Priolo, S.U. Campisano, Phys. Rev. B 53 (1996) 7742-7749.
- [19] C. Spinella, S. Lombardo, F. Priolo, J. Appl. Phys. 84 (1998) 5383.
- [20] R. G. Elliman, J. S. Williams, W. L. Brown, A. Leibereich, D. M. Maher, R. V. Knoll, Nucl. Instr. Meth. B 19/20 (1987) 435.
- [21] J. Linnros, W.L. Brown, R.G Elliman, Mat. Res. Soc. Symp. Proc. 100 (1988) 369.
- [22] R.S. Germanà, S.U.Campisano, Appl. Phys. Lett. 60 (1992) 1726-1728.
- [23] S. Roorda, W. C. Sinke, J. M. Poate, D. C. Jacobson, S. Dierker, B. S. Dennis, D. J.Eaglesham, F. Spaepen and P. Fuoss, Phys. Rev. B **44** (1991) 3702.
- [24] P. A. Stolk, F. W. Saris, A. J. M. Berntsen, W. F. van der Weg, L.T.Sealy, R. C. Barklie, G. Krötz and G. Müller, J. Appl. Phys. **75** (1994) 7266.
- [25] P. Roura, J. Farjas and P. Roca i Cabarrocas, J. Appl. Phys. **104** (2008) 073521.
- [26] D. Turnbull, J.C. Fisher, J. Chem. Phys. 17 (1949) 71-73.
- [27] K. F. Kelton, A. L. Greer, C. V. Thompson, J. Chem. Phys. 79 (1983) 6261-6276.
- [28] K.W. Wang, W.G. Spitzer, G.K. Hubler, D. Sadana, J. Appl. Phys. 58 (1985) 4553-4564.
- [29] J. P. Biersack and L. G. Haggmark, Nucl. Instrum. Methods **174**, 257 (1980)
- [30] L. Colombo, D. Maric, Europhys. Lett. **29** (1995) 623-628.

- [31] W.A. Johnson, R.F. Mehl, *Trans. Am. Inst. Min. Metall. Pet. Eng.* 135 (1939) 416-458.
- [32] M. Avrami, *J. Chem. Phys.* 7 (1939) 1103-1112.
- [33] M. Avrami, *J. Chem. Phys.* 8 (1940) 212-224.
- [34] M. Avrami, *J. Chem. Phys.* 9 (1941) 177-184.
- [35] S.U. Campisano, S. Coffa, V. Raineri, F. Priolo, E. Rimini, *Nucl. Instrum. Methods Phys. Res. B* 80/81 (1993) 514-518.
- [36] R. D. Goldberg, J. S. Williams, R. G. Elliman, *Nucl. Instr. Meth. B* 106 (1995) 242.
- [37] M. Nastasi, J.W. Mayer, J.K. Hirvonen, *Ion-Solid Interaction: Fundamentals and applications*, Cambridge University Press, Cambridge, 1996.
- [38] P.J. Schultz, C. Jagadish, M.C. Ridgway, R.G. Elliman, J.S. Williams, *Phys. Rev. B* 44 (1991) 9118-9121.
- [39] S. Coffa, F. Priolo, and A. Battaglia, *Phys. Rev. Lett.* 70 (1993) 3756-3759.
- [40] F. Priolo, S. Coffa, and A. Battaglia, *Nucl. Instrum. Methods Phys. Res. B* 90 (1994) 314-321.
- [41] S. E. Donnelly, R. C. Birthcher, V. M. Vishnyakov, G. Carter, *Appl. Phys. Lett.* 82 (2003) 1860.
- [42] F. Priolo, C. Spinella, and E. Rimini, *Phys. Rev. B* 41 (1990) 5235-5242.
- [43] G. Mannino, C. Spinella, R. Ruggeri, A. Mio, and E. Rimini, *Mat. Letters* 126 (2014) 28-31.